Automatic reconstruction of serial sections using the finite element method

Elizabeth Guest and Richard Baldock

MRC Human Genetics Unit, Western General Hospital, Crewe Road, Edinburgh EH4 2XU, UK

Submitted 4 December 1995, accepted 26 February 1996

Abstract. Serial sectioning of biological material is often the only way to reveal the 3D structure and function. In this paper we describe a fully automatic method for correcting the sectioning distortions (warping) in order to produce a smooth representative reconstruction of the original object. The basic idea is to attach springs to correspondences established between sections where each section is modelled as a thin elastic plate, constrained so that points can only move within the plane of the plate, and then to let go and wait until the system reaches equilibrium. Correspondences between sections are calculated using new image processing techniques; the finite element method is used to establish the equilibrium position. We show that the warping algorithm described here produces significant improvements over registration and that smoothing of the entire voxel image is achieved.

Keywords: serial sections, reconstruction, warping, matching, correspondence, finite element method.

1. Introduction

In many experiments in biological and medical research, serial sectioning of biological material is the only way to reveal the three dimensional (3D) structure and function. Other 3D imaging techniques such as CT, MRI and confocal microscopy are not always appropriate because they cannot provide the necessary resolution or contrast, the specimen is too large, or the staining techniques require sectioning. Therefore reconstruction from serial sections remains the only method for 3D investigations in many biomedical experiments. Reconstruction is a difficult problem due to the loss of 3D alignment as the sections are cut and, more seriously, the systematic and random distortion caused by the sectioning and preparation processes.

Many authors have reported how serial sections can be automatically registered (Hibbard and Hawkins 1988, Hibbard *et al* 1993, Andreason *et al* 1992, Apicella *et al* 1989, Rydmark *et al* 1992), but there have been only a few studies of automated correction of the sectioning distortions. Reported methods of deformation correction are based on surface smoothing (Deverell *et al* 1993, Gérard *et al* 1993), global (polynomial) transformations (Lamers *et al* 1989, Laan *et al* 1989, Kriete 1989, Olivo *et al* 1993, Jansson 1994), or involve local warping (Dürr *et al* 1989, Verbeek 1992, Montgomery and Ross 1994).

Recent studies on the deformation undergone by the sections as they are processed show that although good results have been obtained by global linear transformations (Laan *et al* 1989, Jansson 1994, Yaegashi *et al* 1987), the deformations are local in nature (Berthold *et al* 1982, Jones *et al* 1994). These studies show that the deformation depends on a variety of factors including the type of tissue and embedding material. Therefore, and because a local warp function will also describe all other kinds of transformation, a deformation correction method should calculate the warp function locally for each part of the section.

With the exception of the methods based on surface smoothing, and that proposed by Montgomery and Ross (1994), all reported methods match each section to only one adjacent section, and are designed to warp one section so that it matches the other exactly. To provide a reconstruction which reproduces the original (unsectioned) object, methods which warp images of cut sections (diascopic images) onto images of sections before they were cut (episcopic images) (Lamers *et al* 1989, Laan *et al* 1989, Verbeek 1992) are required. However episcopic images are

0966-9051/95/040154+14$19.50

not always available and may be difficult to provide for long series of sections.

In this paper we describe a fully automatic method for warping serial sections in order to produce a smooth *representative* reconstruction of the original object. This is required to reconstruct mouse embryos at different developmental stages which will form the basis of an atlas of mouse development (Baldock *et al* 1992, Ringwald *et al* 1994). We do not aim to reproduce the original unsectioned object, but to generate a representative example of the mouse embryo. To produce a smooth progression from the first to the last section it is important that the warp calculation for each section obtains information from both adjacent sections, and that this information is updated as these sections are warped. This is the approach taken by Montgomery *et al*, but their method requires that contours are manually extracted, and includes no connectivity information between contours on the same section, thus requiring the use of *ad hoc* criteria to prevent excessively large warps.

The solution to the warping problem described in this paper is to model each section as a thin elastic plate constrained so that points in the plate can move only within the plane of the section. Correspondences between sections are established by pattern matching and are used to generate forces which act on each section and are modelled by springs attached to points in adjacent sections. The finite element method (FEM) is used to find an equilibrium position for the stack. This approach ensures that the warp function defined over each section is continuous and large deformations can be controlled (or prevented) by using appropriate material properties and external constraints (thus preventing, for example, a sphere being warped into a cylinder).

In the subsequent sections we discuss the mathematical model used to model each section as a thin elastic plate, and how the FEM can be used to calculate an equilibrium for each section. Since the problem of warping the entire stack is too large to solve directly, an iterative technique has been developed. To test the warping algorithm and to measure its performance with respect to model parameters, a new measure of the quality of a reconstruction is defined and the results of experiments to test and evaluate the behaviour of the algorithm are presented.

2. Methods

2.1. Mathematical modelling

To warp a stack of sections, each section is modelled as a thin elastic plate. To each plate we apply forces, obtained by matching adjacent sections, and, for simplicity, modelled as springs†. Initially the internal stresses are zero and therefore the system is not in equilibrium. To find the equilibrium displacements we minimize the energy functional (Rees 1990, Richards *et al* 1960)

$$\mathcal{E} = \frac{1}{2}\int_V \boldsymbol{\sigma}^T \boldsymbol{\epsilon} dV + \frac{1}{2}\sum l_i^2 k_i, \tag{1}$$

where $\boldsymbol{\sigma}$ is the stress vector, $\boldsymbol{\epsilon}$ is the strain vector, k_i is the spring constant of spring i, l_i is the extension of spring i, and the integration is over the volume of the current configuration of the section.

The energy functional is a non-linear equation for the displacement field because the integration volume depends on the displacements and the material constitutive relations may be non-linear. There are two main ways of numerically minimizing this equation: either convert it to a differential equation (Euler Lagrange theory) and use finite differences, or use the finite element method (FEM). In the FEM the domain is divided into finite elements (regions of the 2D plane) which can be of any size or shape, and *shape functions* are defined over each element so that the values of the function inside the element are defined by its values at the nodes. The problem is then reduced to that of finding the values at these nodes and the original equation is reduced to a set of simultaneous equations which can be solved using standard techniques.

In this work we use the FEM because it is easier to apply to problems with non-linear constitutive relations and arbitrary internal and external constraints. In particular:

(i) The elements in the FEM can be of any shape, and need not all be the same size so that the resolution of the elements can be decided by the accuracy required for different parts of the image.
(ii) Each element in the mesh can be assigned different material properties. For example the object of interest can be made stiffer than the background.
(iii) The FEM allows arbitrary constraints or boundary conditions such as fixed points or lines to be added or deleted simply.

2.2. The FEM

We now outline the essentials of using the FEM to calculate the equilibrium position of each section. Further details may be found in Bathe (1982), Stasa (1985), Zienkiewicz and Taylor (1989, 1991). Since the integration in the energy functional is over an unknown volume, we use stress and strain measures that transform the stress and strain in the warped configuration to the original configuration (Bathe 1982). These are most conveniently expressed using tensor notation and we define the second Piola–Kirchhoff stress tensor at time t referred to configuration 0 (at time 0) by

$${}^t_0 S_{ij} = \frac{{}^0\rho}{{}^t\rho}\, {}^t_0 x_{i,m}\, {}^t_t \sigma_{mn}\, {}^t_0 x_{j,n} \tag{2}$$

† Although the forces are modelled as springs, there is no loss of generality as the spring constants can be modified at each (finite element) iteration to reproduce any required force behaviour.

where ${}^t\rho$ is the mass density at time t, ${}^t_t\sigma_{mn}$ is the engineering stress at time t (referred to configuration t), and ${}^t_0x_{i,m}$ is a member of the deformation tensor. The strain tensor to be used with the second Piola–Kirchhoff stress tensor is the Green–Lagrange strain tensor. This is defined at time t, with reference to time 0 by

$$ {}^t_0G_{ij} = \tfrac{1}{2}({}^t_0u_{i,j} + {}^t_0u_{j,i} + {}^t_0u_{k,i}\,{}^t_0u_{k,j}) \qquad (3) $$

where ${}^t_0u_{i,j} = \partial^t u_i/\partial^0 x_j$. Here ${}^0x_i$ $(i = 1, 2)$ gives the coordinates of a point in the plate at time 0, and ${}^tx_i = {}^0x_i + {}^tu_i$ gives the coordinates of the point at time t. Both the second Piola–Kirchhoff stress tensor and the Green–Lagrange strain tensor are symmetric and invariant to rigid body transformations.

Using these stress and strain tensors, the above energy functional can be written as

$$ \mathcal{E} = \frac{1}{2}\int_{{}^0V} {}^{t+\Delta t}_0S_{ij}\,{}^{t+\Delta t}_0G_{ij}\,{}^0\mathrm{d}V + \frac{1}{2}\sum l_i^2k_i. $$

For equilibrium we minimize this energy by setting the first variation to zero:

$$ \int_{{}^0V} {}^{t+\Delta t}_0S_{ij}\,\delta{}^{t+\Delta t}_0G_{ij}\,{}^0\mathrm{d}V + \sum l_ik_i\delta l_i = 0. \qquad (4) $$

The method of finite elements discretizes this equation by dividing the spatial domain into small discrete regions (elements) and assumes a known 'shape function' within that region. The shape function is defined in terms of the function values at the element nodes.

The material properties used for warping were those of a compressible hyper-elastic material with strain energy function of the form

$$ W(\lambda_1, \lambda_2) = u_1(\lambda_1^{\alpha_1} + \lambda_2^{\alpha_1} - 2)/\alpha_1 + u_2(\lambda_1^{\alpha_2} + \lambda_2^{\alpha_2} - 2)/\alpha_2, $$

where λ_i are the principal stretches and u_i and α_i are constants (set to $u_1 = 1$, $u_2 = -1$, $\alpha_1 = 4.5$ and $\alpha_2 = -2.0$). See Ogden (1984) for details of the incremental constitutive matrix obtained from these material properties, and Bathe (1982) for details of how to include this in the FE equations.

The strain tensor, ${}^t_0G_{ij}$ is a non-linear function of the displacements. Therefore to use this expression within the finite element formulation it must be linearized and the solution found by iteration. This iteration will converge when the initial approximation is sufficiently close to the correct solution. The standard technique to satisfy this condition is to start at time 0 with a small load, and increase the load at each time step until the desired loading is reached. In this paper we use an alternative mechanism which is to limit the nodal displacements for each iteration; this is similar to damping the dynamic solution. The displacement constraint is that the dimensionless quantity

$$ q_e = \frac{\max_i d_{ei}^2}{a_e} < 0.5 $$

where d_{ei} is the displacement of each node i of element e and a_e is the area of the element. This iteration is termed *finite element iteration*.

The inter-section forces are established by matching but after each section is warped the match results may change, therefore it is necessary to include an additional level of iteration, termed *force iteration*, to account for this effect.

In the above, we have assumed that the springs are attached to points. However, since correspondences are often calculated by matching edges, the springs were attached to infinite lines and allowed to slide along these lines with zero penalty. In practise, to avoid numerical instability, each spring is attached to the nearest point on its corresponding line, and the attachment point is updated for each FE iteration. In this way the points are allowed to slide freely along their corresponding lines as the FE iteration progresses.

So far we have shown how the finite element method can be used to warp a single section, but the final configuration of each section depends on the warp of the adjacent sections. In principle, the method could be used to warp the whole stack in one step, but this is computationally infeasible and we therefore find the required equilibrium position by *stack iteration*. We have investigated two schemes for warping the whole stack:

(i) Warp each section consecutively using the most recent information for adjacent sections and reversing the direction of warping for each pass through the stack.
(ii) Split the stack iteration into two passes: the first warping all odd numbered sections; the second all even numbered sections. In each pass, the most recent warp information is used.

Iteration scheme 1 propagates warp information immediately, and the iteration in both directions compensates for the directional propagation. In iteration scheme 2, warp propagation may be slower but is symmetric, and has the advantage that it is simpler to run in parallel. We have tested both options (see Guest (1994) for full details) and find that both converge equally well but that in application to real data (50 sections), scheme 2 is nearly three times faster. This is very significant because some of the calculations may require 72 cpu *hours* or more on a SPARC 10/41. Most of this time (93.4%) is spent doing image processing which will be described in section 2.4; only 6.6% of the time is spent doing FE analysis (Guest 1994).

2.3. Calculating the finite element mesh

In our application we are interested in the warp of the 'foreground' or object pixels. In order to make the calculation faster (fewer elements) and yet respond to the image content we have developed an algorithm which will triangulate each section automatically with a higher element density over the "interesting" parts of the image. The basic idea is to determine a set of points to act as nodes for

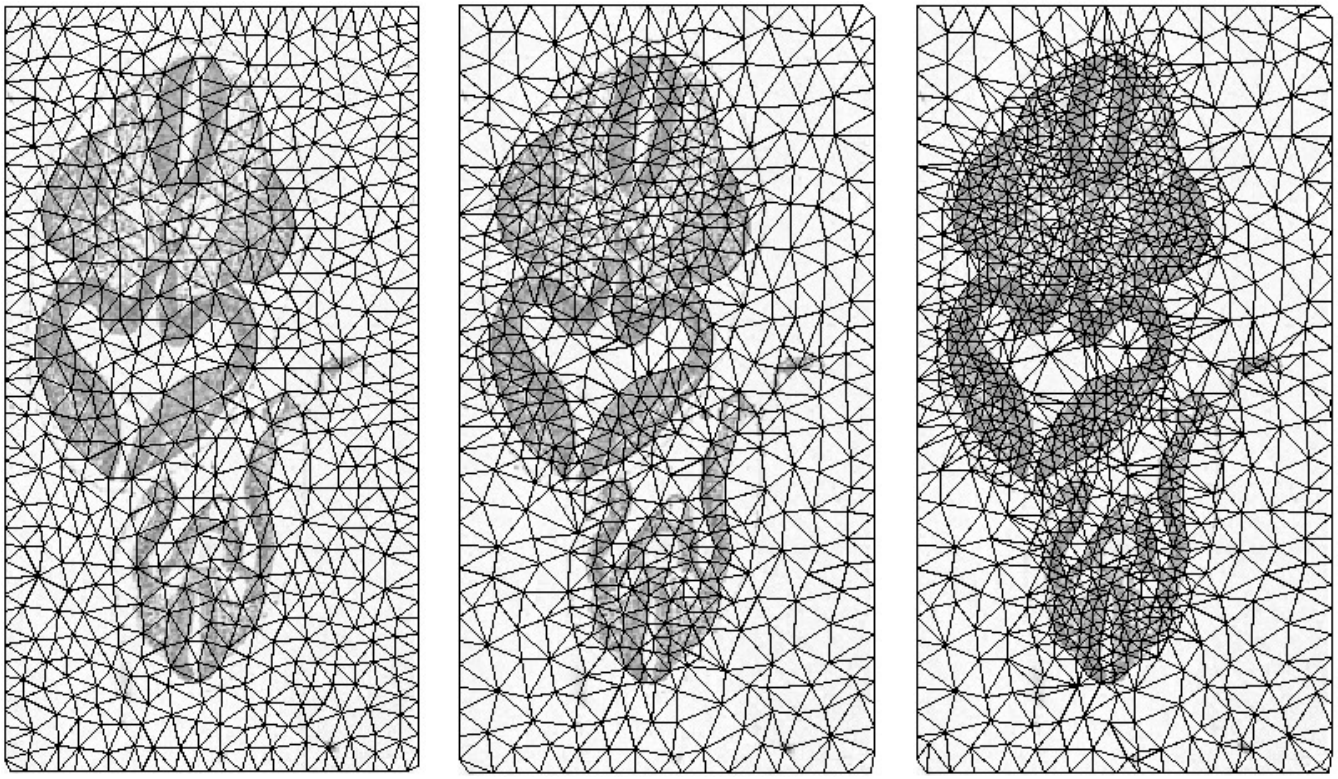

Figure 1. The finite element mesh for an image in the 9 day mouse embryo series with three sets of distance parameters: d1 is the minimum nodal separation for the object; d2 is the minimum nodal separation for the background.

the elements with high density over the region of interest, and then to calculate the Delaunay triangulation to find the actual elements. The Delaunay triangulation avoids long thin triangles and makes the triangles as regular as possible (Preparata and Shamos 1985).

Ideally we would like the nodes to be located along the structural edges so that the boundaries on the triangles will tend to follow the boundaries of the regions. These points should be located at points of maximum curvature to fully describe the shapes of the regions. However we also require points in the middle of the regions to ensure a fine mesh with higher density over the domain of the object. The algorithm employed is:

(i) Calculate the modulus of the image gradient (derivative of Gaussian of half-width at half-maximum of 1.0 pixels).
(ii) Threshold the gradient image at a value removing the background peak of the histogram†.
(iii) Order the points above threshold by gradient value and, starting from the highest value, points are chosen subject to not being too close (defined by distance d1) to a previously selected point. This produces a scatter of points over the object. Since higher valued points are chosen first, the first points chosen are more likely to be located on boundaries of regions.
(iv) Repeat (iii) for the background region using a larger minimum distance (d2).
(v) Calculate the Delaunay triangulation from the list of nodes (Lee and Schachter 1980)‡.

Figure 1 shows the result of this algorithm for a number of minimum distance values. Note that if the image is such that an equally fine mesh is required over the whole image, the two nodal separation distances can be equal.

To determine the warped image from the warped mesh, we scan though all the pixels in the warped domain and establish the coordinates of the corresponding point in the original image. For this we need to know the element in which each point lies as we are scanning through the warped mesh. An efficient way of scanning the warped mesh while keeping track of the position of the points with respect to the mesh is the *plane sweep technique* (Preparata and Shamos 1985).

† It was found that the object is characterized by high gradients while the background is characterized by low gradients. The threshold value is estimated from the histogram by finding the most distant point from the chord from the histogram peak to the highest value.

‡ The authors wish to thank Glynn Robinson (Department of Diagnostic Radiology, Yale University) for his implementation of this algorithm.

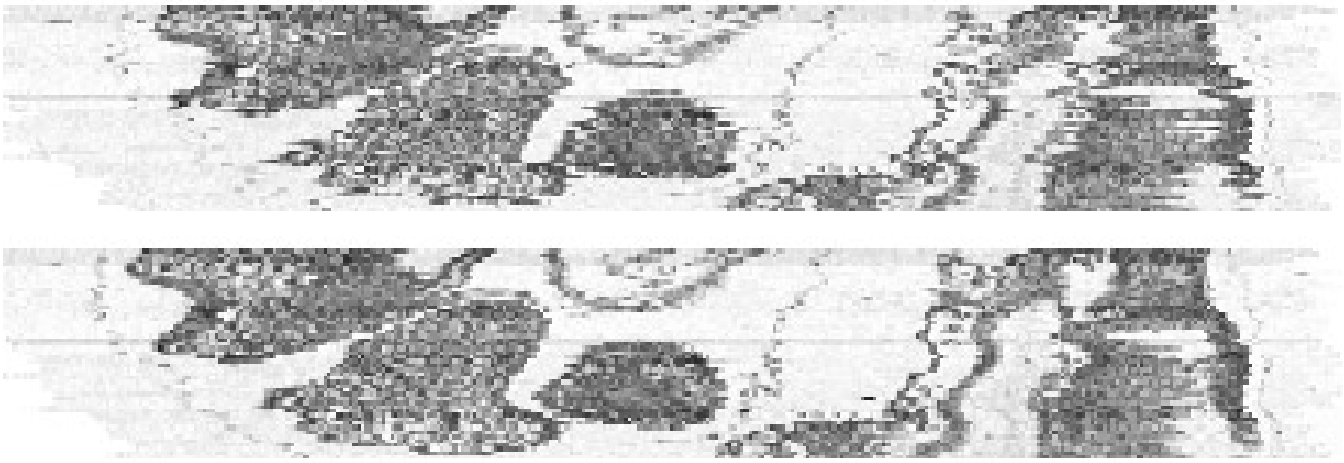

Figure 2. The results of warping 50 sections of the 9 day series. The top image shows the registered stack; the bottom image shows the results of warping the registered stack.

2.4. Matching and calculating correspondences

It is essential that the forces arising from correspondences between adjacent sections are calculated fully automatically. Because it is impossible to ensure that every proposed correspondence is correct, we require a matching algorithm which will provide the current best match and an estimate of the confidence of the match. The match point determines the spring end point; the confidence determines the spring strength. The strategy is to select a number of points according to their edge strength, these are termed 'interesting points'. To each of these points is attached a spring linking it to corresponding points in the adjacent sections. The correspondences and the strength of each spring are determined by matching. More details of the algorithm described below will be found in Guest 1994).

The matching is based on statistical tests on populations of pixels either side of an hypothesized line. The attributes of each population used for this test are the mean and standard deviation and therefore an appropriate statistic is the F-test (Erricker 1971) and the line direction is that which maximizes the F-test value. In this work we test a finite set of line directions by using a series of masks and select the maximum. The filter response can be predicted and in principle a better estimate of the line direction is available by fitting the response of all hypothesized directions with the appropriate curve but this has not proved necessary in this case.

We match image points from two images, A and B, by calculating a measure of similarity between two regions R_{A_1} and R_{B_1} and between regions R_{A_2} and R_{B_2}, defined on either side of the hypothesized line of the points in images A and B respectively. We require that the match function gives a high value if each of the two pairs of regions have similar means and variances and the edge directions are similar.

We require a match or cost function to provide a tunable response to differences in the mean and variance between two image regions. Since the T-statistic (Erricker 1971) compares the means and the F-statistic compares the variances, we have tested the tunable function $\mathrm{F}^{\alpha}\mathrm{T}^{\beta}$ for our application, where T and F are the T- and F-tests applied to R_{A_1} and R_{B_1} or to R_{A_2} and R_{B_2}. This must be combined with a similar test for the other pair of regions into a function which has output values in the range [0, 1], such that a perfect match yields 1 and smaller values result from poorer matches. We choose the simple functional form

$$f = [1 + \mathrm{F}_1^{\alpha}\mathrm{T}_1^{\beta} + \mathrm{F}_2^{\alpha}\mathrm{T}_2^{\beta}]^{-1}$$

to satisfy these criteria, where F_i and T_i refer to the F- and T-tests applied to R_{A_i} and R_{B_i}.

The overall match function must also include the difference in the directions of the hypothesized edges of the two image points. For this we assume that the expected line direction is normally distributed about the test line direction and that this term is independent of the grey level statistics. Therefore our match function is

$$m = f \times \exp\left[-\left(\frac{|\theta_1 - \theta_2|}{\omega}\right)^2\right].$$

The parameter ω should be chosen so that a small angle penalty is calculated for differences in angles up to the resolution of the line direction calculation (a value of 30 degrees was found to be suitable for 5×5 masks); the parameters α and β were set to $\alpha = 1$ and $\beta = 2$ by experiment.

Calculating correspondences with suitable confidence is difficult due to the conflicting requirements of correspondence and warping. Since algorithms for automatically registering sections exist (Hibbard and Hawkins 1988, Hibbard *et al* 1993, Apicella *et al* 1989, Andreason *et al* 1992, Rydmark *et al* 1992), we may assume that the sections are registered and that therefore the search for correspondences can be restricted to local

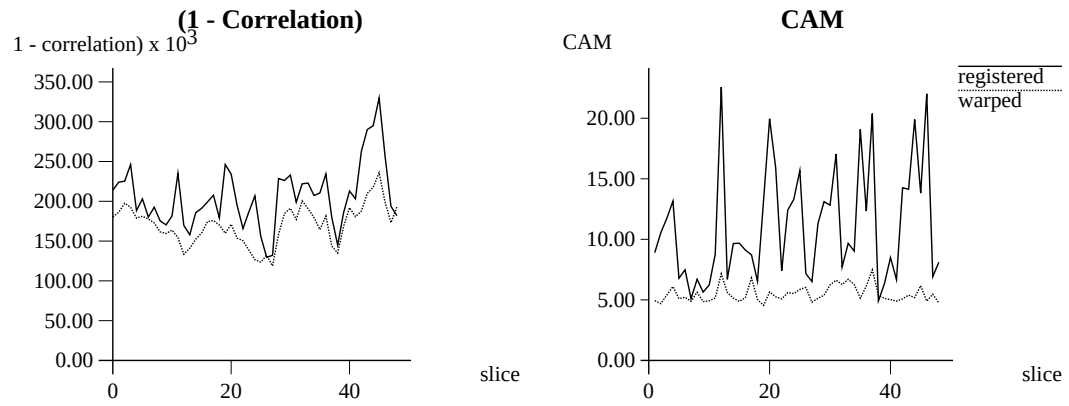

Figure 3. Graphs showing the values of $(1 - correlation)$ and the CAM for a registered and warped stack of sections.

neighbourhoods. Thus we require that more weight be given to closer and better matches as these are more likely to be correct. For warping we assume that given three corresponding points, one on the section to be warped, and one on each of the two adjacent sections, the desired position of the point on the middle section is midway between the positions of the other two points. To achieve this, forces applied by more distant correspondences must be stronger than those applied by closer correspondences. This behaviour is achieved by modelling the forces as springs where the spring constants depend on the confidence that the correspondences are correct.

The match confidence which determines the spring constant is calculated by testing the robustness of the match to small spatial movements of the interesting point. If the correspondence is clear and unambiguous, moving the interesting point should result either in no change in the position of the calculated correspondence point or in a change along the local edge. Therefore a set of 'tentative corresponding points' obtained by moving the interesting point within a small neighbourhood of its original position will be a single point or line when there is a strong match†, or a scatter of points when there is a weak or ambiguous match. To establish the match confidence, a straight line is fitted to the points and the sum of squared distances from the line is calculated. This is converted to the range [0, 1] using an appropriate Gaussian transformation with parameters set by experiment.

2.5. Evaluation criteria

Objective evaluation of the results of warping a stack of images is difficult. The methods used in the literature for comparing registration algorithms (Santori and Toga 1993, Toga and Banerjee 1993) include:

- visual evaluation of a cross section through the stack,
- visual evaluation of adjacent sections by superposition,
- cross-correlation, and
- analysis of the positions of tie points.

Visual evaluation is subjective and a significant number of sections have to be warped before a visual analysis of the cross section has any value (so that a reasonable image is produced). In addition, if only small differences are visible it can be difficult to discriminate between the results. Superpositioning adjacent sections can give a good indication of how well two particular sections have been brought into alignment, but no indication of how well the whole stack has been reconstructed. The only objective evaluation criteria used in the literature are the mean and standard deviation of the image correlation of adjacent sections, and the absolute differences from the mean position of a number of tie points. Both of these measures are logically flawed for this purpose because their extremum values correspond to *exact* matching and therefore cannot reflect the true 3D structure (which we are trying to reconstruct).

An ideal measure of the quality of a reconstruction (for this application) would measure the smoothness of the reconstructed surfaces. A fully automatic implementation of this would be difficult because of the difficulties of reliably segmenting surfaces from 3D data. We approximate the smooth surface constraint by assuming that if a point is perfectly aligned, it lies midway between its corresponding points on adjacent sections. This is reasonable because the points selected for matching tend to lie on structures which vary slowly compared to section thickness. Since embryological surfaces meet these constraints most of the time, a measure based on the sum of the displacement vectors from a point to its two corresponding points on adjacent sections should give an estimate of the quality of a reconstruction.

The new measure based on this approach is as follows: for all pixels in the image, calculate the corresponding points and associated confidences in both adjacent images.

† In practice, since the algorithm for finding interesting points is based on the F-test filter, which is a type of edge filter, only lines are considered. However, if a method for locating and matching points were implemented, points would also be considered.

Table 1. Table showing the correlation and CAM values for the 5 stacks of experiment 2 before and after warping. The correlation shown is $(1 - correlation)$.

	1 - correlation					
	registered		warped		CAM	
	mean	std	mean	std	registered	warped
stack 1	0.151	0.213	0.209	0.094	14.932	8.766
stack 2	0.188	0.266	0.271	0.197	20.260	12.423
stack 3	0.219	0.310	0.299	0.205	16.310	14.263
stack 4	0.179	0.253	0.302	0.113	15.402	8.386
stack 5	0.215	0.303	0.288	0.167	23.075	11.336

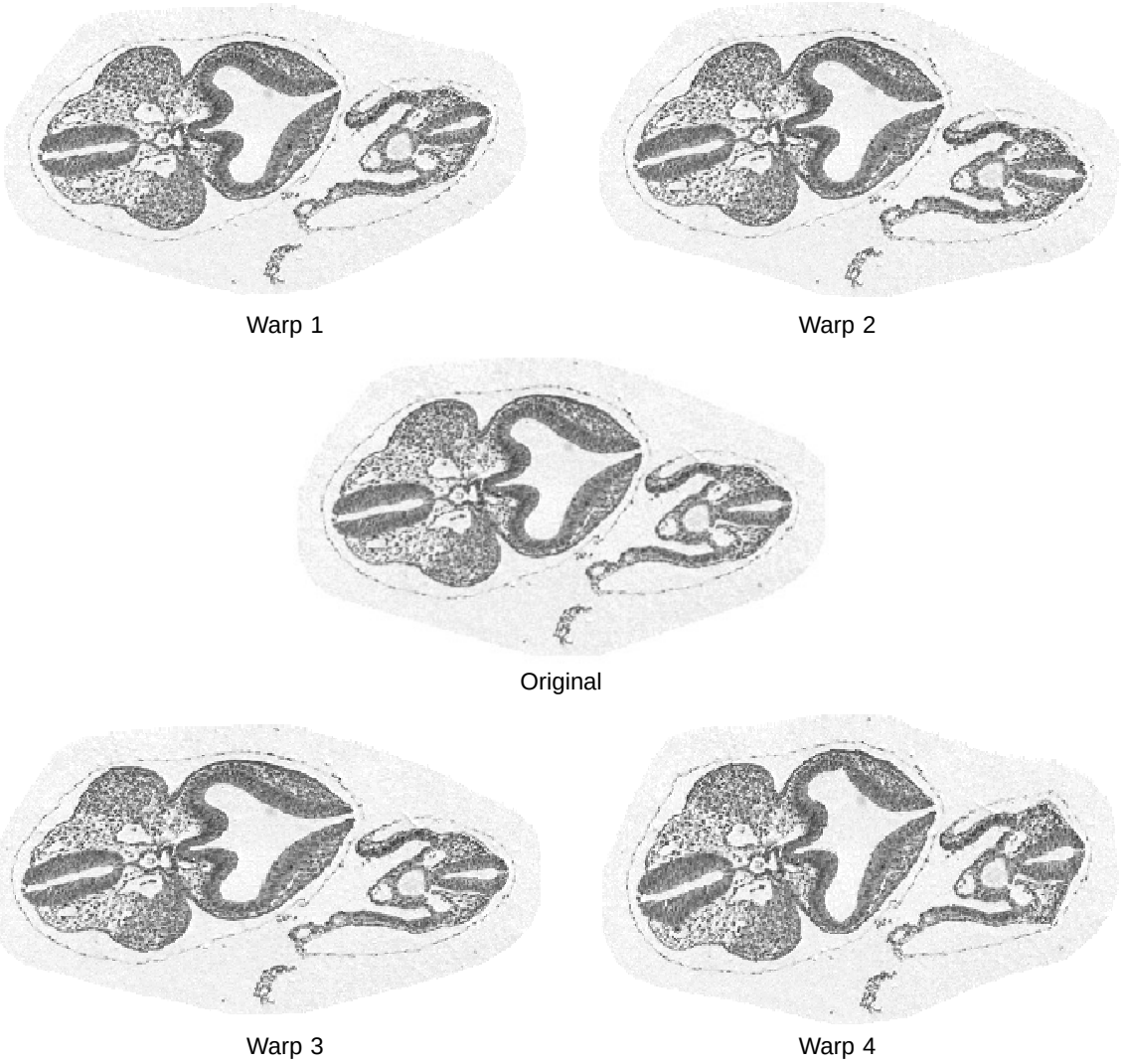

Figure 4. The four warps applied to one of the test images.

If the confidence is greater than a threshold, calculate the sum of the vectors and add the square of the resultant to the cumulative sum. The cumulative sum is normalized by the number of pixels which have contributed. This new measure will be referred to as the correspondence alignment measure (CAM) and experiments below show that it is more suitable than correlation for comparing the qualities of two reconstructions.

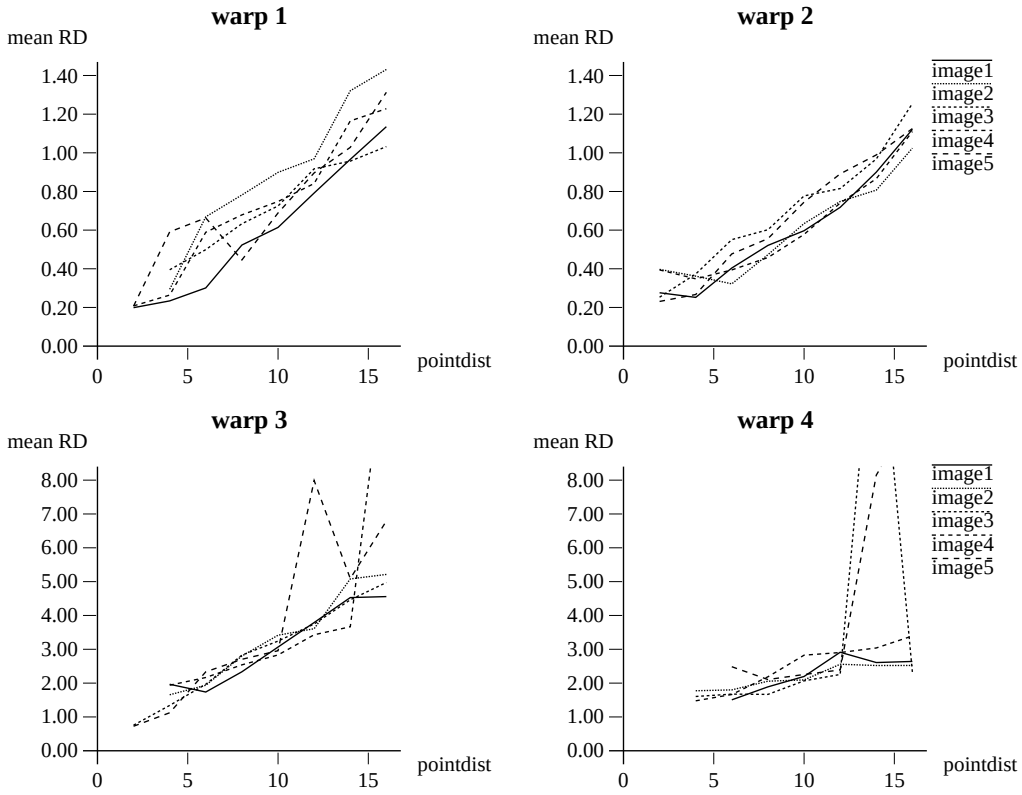

Figure 5. Graphs showing the results of the effects of varying **pointdist**.

Finally we note that the CAM gives a value for each section. In order to compare reconstructions as a whole we will compare the mean and standard deviation of this value over the whole stack.

3. Experiments and results

To test the CAM and performance characteristics of the warping algorithm we used serial sections of a 9-day mouse embryo cut by Kaufman for the paper atlas of mouse development (Kaufman 1992). The embryo was embedded in paraffin wax, sectioned at 7 μm and stained with haematoxylin and eosin. The sections were digitized at a resolution of 2.2 μm, corrected for shading and subsampled to half the original resolution. The series consisted of 307 sections.

To evaluate the results of the experiments on test images, where the required warp is known, we will analyse the residual displacement

$$\mathrm{RD} = \sum_{\text{all pixels}} (\text{applied displacement}) + (\text{calculated displacement}).$$

The results of experiments on stacks of images will be evaluated using visual criteria and the CAM.

3.1. Evaluation measure (CAM)

The relative usefulness of image correlation,

$$C(I_1, I_2) = \frac{I_1 \odot I_2}{\sqrt{(I_1 \odot I_1)(I_2 \odot I_2)}}, \qquad I_1 \odot I_2 = \sum_{i,j} I_1(i,j) I_2(i,j), \tag{5}$$

and the CAM cannot be evaluated analytically for a particular application and a set of experiments was designed to highlight their differences.

3.1.1. Experiment 1 Correlation and CAM values were calculated for each image of a registered stack of images, and a warped stack of the same images which is clearly better in terms of visual criteria. The stack used was a stack of 50 alternate sections chosen from the middle of the 9 day mouse embryo series and registered using the method described by Hibbard *et al* (1988). A section through the registered and warped stacks is shown in figure 2. Note that the warping algorithm has had the required effect on the 9 day series in that the boundaries of structures are more clearly defined.

The results of calculating correlation and the CAM for both the registered and warped stacks are given in figure 3 which shows the values of (1−*correlation*) and the

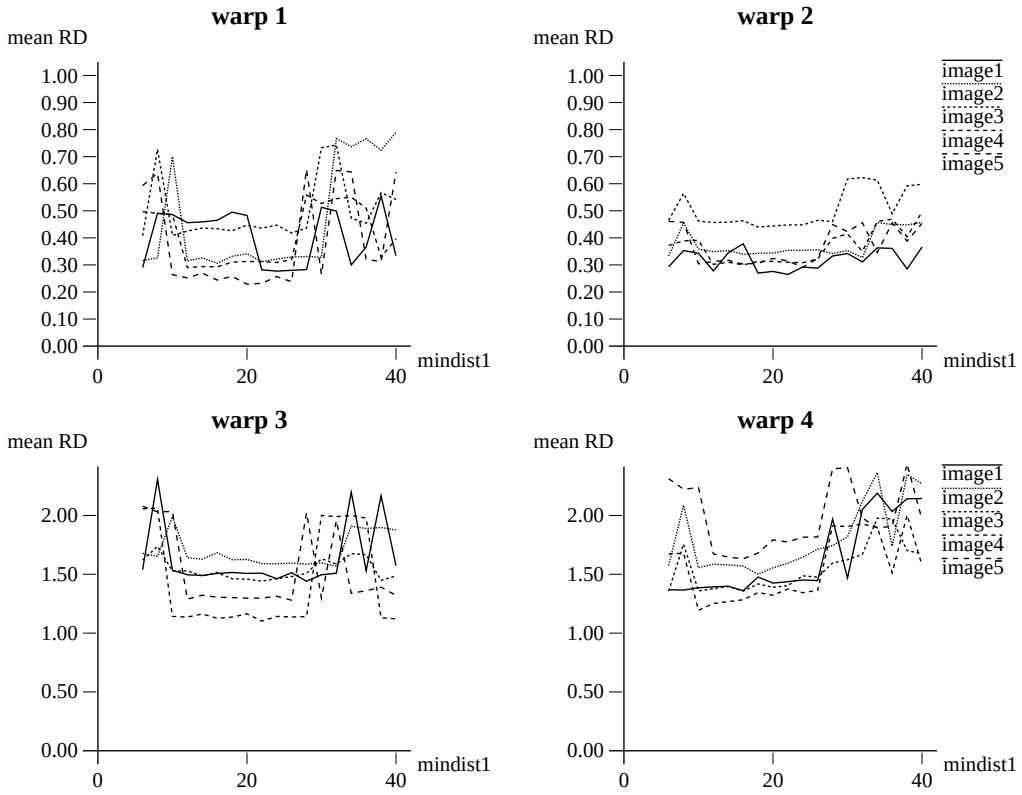

Figure 6. Graphs showing the results, for the first set of test images, of the effects of varying the resolution of the finite element mesh.

CAM for each section in the registered and warped stacks. From these graphs we see that the values for the warped stack have lower means and vary less than those for the registered stack although the values for isolated sections may be worse. The difference in the mean and standard deviation is most noticeable for the CAM. In fact the mean values have dropped by 15.3% and 50.6% and the standard deviation by 36.6% and 85.9% for $(1 - \textit{correlation})$ and the CAM respectively.

3.1.2. Experiment 2 Five images were chosen at intervals of approximately 25 sections from the middle of the 9 day series and a stack of three sections was generated from each of these sections. In each stack, the first two images were copies of one of the chosen sections and the third image was chosen so that it was adjacent but one in the series to this section. $(1 - \textit{correlation})$ and the CAM were evaluated for the middle section of each stack relative to the first and third sections before and after warping, and the results are shown in table 1. For $(1 - \textit{correlation})$, we see that in all cases the mean has increased with respect to both adjacent sections, but the standard deviation has decreased. The results for the CAM show that in all cases this has decreased, showing that the overall alignment has improved.

From this experiment we conclude that the mean $(1 - \textit{correlation})$ value is not a reliable measure as it decreases when a section resembles one of its adjacent sections more than the other. Furthermore, the standard deviation of correlation is also a poor measure as this remains zero when the middle section of a stack of three identical sections is transformed. In this case the CAM increases and we conclude that the CAM is a more appropriate measure for determining the success of the warping process.

3.2. Reconstruction parameters

The reconstruction algorithm presented in this paper is designed to remove sectioning distortions fully automatically. The experiments reported in this section are to determine how the various parameters affect the final result, and to determine how the algorithm can be improved. The parameters tested were:

(i) the strength of the springs given certain material properties (**springk**),
(ii) the effect of changing the search area for calculating correspondences ($2 \times$ **areasize** $+ 1$),
(iii) the number and spacing of the 'interesting' points (**pointdist**), and
(iv) the resolution of the finite element mesh (**mindist1** and **mindist2** for finer and coarser parts of the mesh respectively).

Five images were chosen at intervals of approximately 25 sections from the middle of the 9 day mouse embryo series.

Table 2. Table showing the values of **mindist1** and **mindist2** used in experiment 4.

mindist1	2	4	6	8	10	12	14	16	18	20
mindist2	4	8	10	12	14	14	14	16	18	20
mindist1	22	24	26	28	30	32	34	36	38	40
mindist2	22	24	26	28	30	32	34	36	38	40

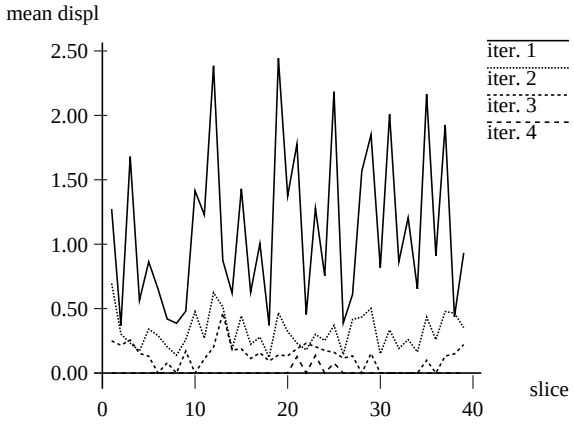

Figure 7. Graph showing the mean displacement for each iteration.

By manually attaching springs, four different warps (see figure 4) were generated and applied to each image to yield twenty test images. Each image was sandwiched between two copies of the original and the warping algorithm was applied for different values of the warping parameters as described below (the top and bottom sections were fixed).

Spring constant. The spring constant (**springk**) and search area (**areasize**) parameters are related since a larger search distance will give rise to more distant corresponding points which will result in stronger forces being exerted by the springs. It is important to employ appropriate values for the spring constants with respect to the material properties as values which are too low will cause the warp to be limited by the elastic properties of each section i.e. the sections resist change), and if the forces are too strong with respect to the material properties, the true shape changes will be smoothed into a linear progression between the top and bottom sections (or whichever sections are fixed)†.

The aim of this experiment was to determine maximum values for the spring constant for each search area, and to test whether high values of **springk** and **areasize** are more successful at warping the image back to the original. For each **areasize** of 5, 10, 15 and 20 pixels, **springk** was set to 0.5, 1, 2, 4, 6, to 20. This experiment was performed on test images.

† At least one section must be fixed to provide boundary conditions for the warping process.

It was found that the mean RD decreases hyperbolically as **springk** increases, giving little improvement in the results for values greater than 10. Although the maximum displacement for the warps was 35 pixels, a search area of 21×21 pixels was adequate in all cases; a search area of 11×11 only failed to give good results for warp 4. From this we conclude that as long as both parameters are sufficiently large, the actual values do not greatly affect the quality of the reconstruction.

Density of interesting points. It is to be expected that the warp will be more accurate if there are more interesting points. To test this **pointdist** was set to 2, 4, 6, to 16 and the test images were warped.

The results of varying **pointdist** are given in figure 5. From these graphs we see that the mean RD increases as the minimum distance between the interesting points increases. Furthermore, for warps 1 and 2, and for the lower values of **pointdist** for warps 3 and 4, this relationship is linear, but as the values of **pointdist** increase, significantly larger errors are observed for some images and some values. Since it is computationally expensive to match large numbers of interesting points, we conclude that **pointdist** should be chosen to ensure sufficient accuracy and for these images a value of **pointdist** $= 7$ is appropriate.

Mesh resolution. The finite element method gives numerically more accurate results (with respect to the stress and the strain) when the finite element mesh is finer. To see what effect this has on the calculated warp, **mindist1** and **mindist2** were tested with the values shown in table 2. From the table we see that **mindist2** is greater than **mindist1** for values up to **mindist1** $= 14$. This was to allow convergence of the finite element method for these higher resolutions.

Since the test images have undergone a global warp, this experiment was repeated on another set of five stacks, each of which contained three images. The first and third images were identical and the middle section in each stack was an adjacent section but one in the series to the identical images. These images were chosen from the middle of the 9 day series at intervals of approximately 25 sections.

Figure 6 shows the results of varying the resolution of the finite element mesh for the first set of test images. From these graphs we see that the resolution of the mesh has no strong systematic effect on the accuracy of the result, although the CAM does increase significantly with respect to the mesh resolution over the test range. The results for the second set of images were similar.

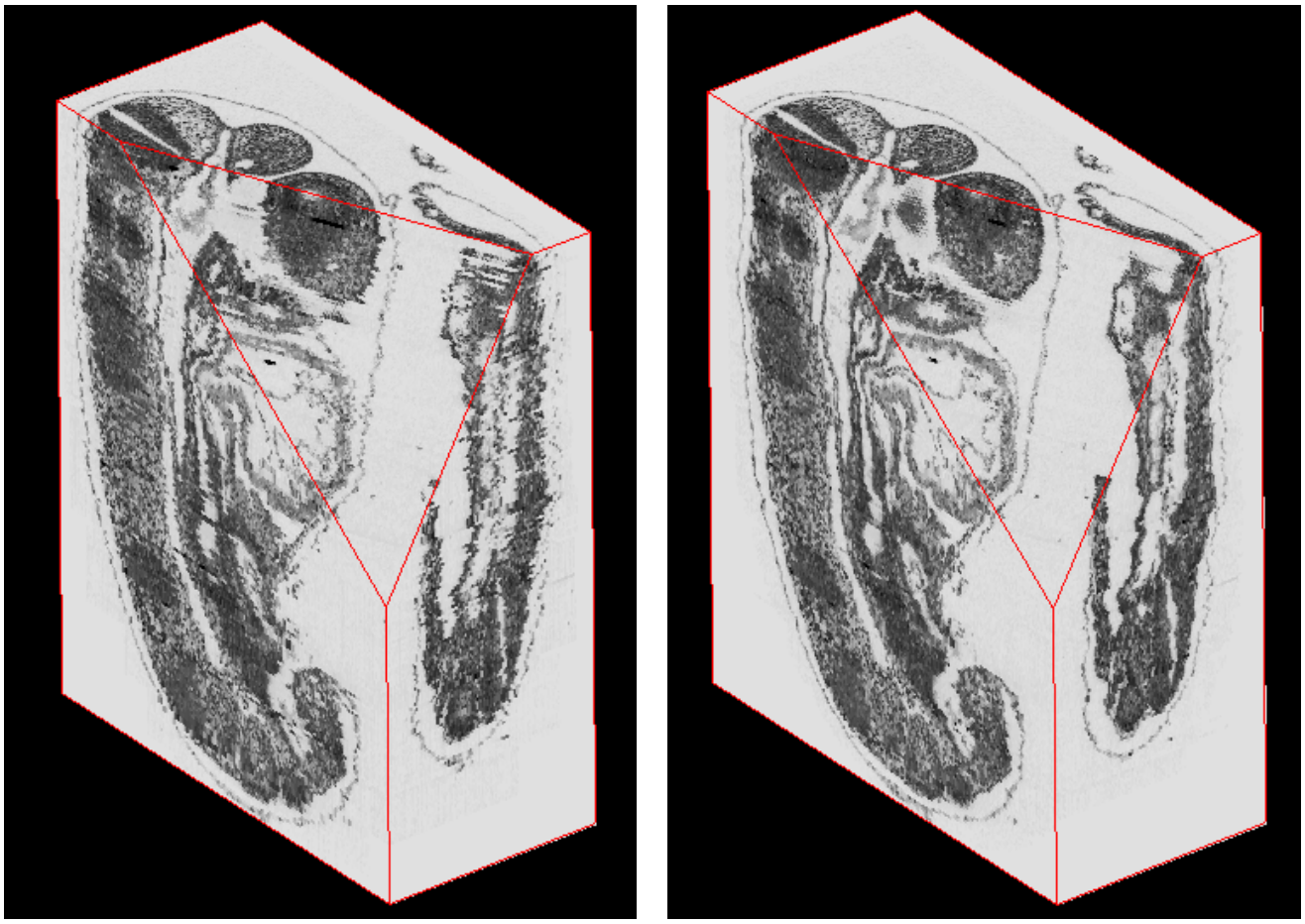

Figure 8. Images of a (manually registered) 9 day mouse embryo before (left image) and after (right image) warping. The top surface of each block shows a section taken in the original cutting direction; the other surfaces show orthogonal sections and a section cut in an arbitrary direction.

Table 3. Table showing the values of the correspondence alignment measure after each iteration.

iteration	mean	std
registered	11.119 523	4.779 772
iteration 1	5.720 964	0.784 895
iteration 2	5.595 593	0.705 386
iteration 3	5.537 617	0.679 738
iteration 4	5.547 075	0.682 444

3.3. Convergence

40 alternate sections were selected from the middle of the 9 day mouse embryo series and were registered using the algorithm described by Hibbard *et al* (1988). Alternate sections were chosen to increase the range of variation in the image content.

The results of calculating the CAM as the sections are warped are given in table 3 which shows that except for the last iteration, the alignment of the images improves with each iteration. Although the results for the last iteration seem to indicate a slight deterioration in quality of the reconstruction, this deterioration is not significant and is probably due to the interpolation algorithm used (nearest neighbour) for calculating the warped images. Visual inspection of the reconstruction shows significant improvement after the first iteration, but there was little difference after subsequent iterations.

Figure 7 shows the mean displacement for each section for each iteration. We see that the mean displacements decrease for each iteration, and that the most dramatic decrease occurs after the first iteration. The maximum and standard deviation of the displacements clearly decrease in a similar fashion.

3.4. Full reconstruction

The warping algorithm was applied to the full 9 day series and a 7.75 day mouse embryo. The 7.75 day embryo was embedded in plastic (araldite), sectioned at 2 μm, digitized at a resolution of 0.68 μm and resampled by a factor of 3. The parameters used for warping the 7.75 day series were 3,

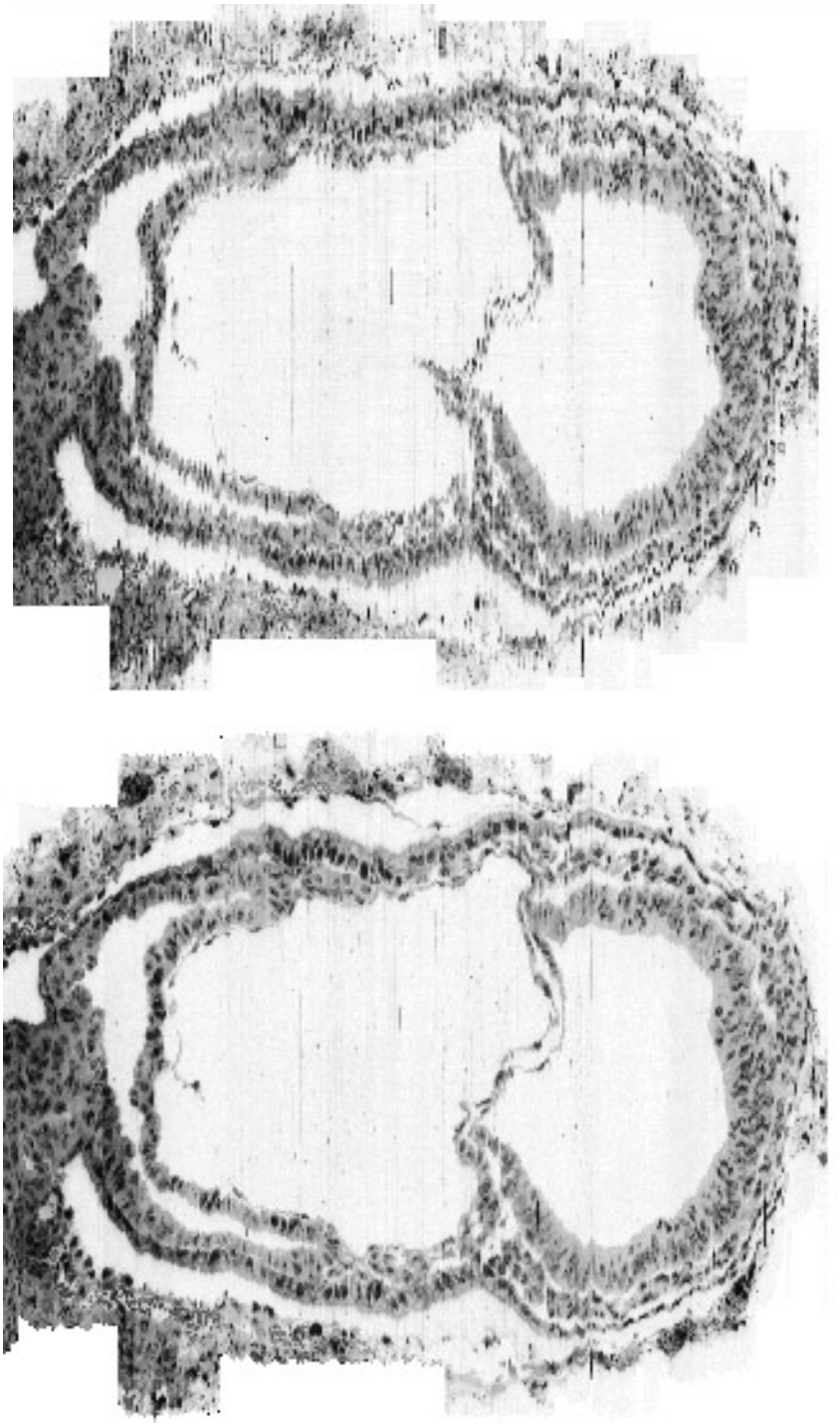

Figure 9. Images of a (manually registered) 7.75 day mouse embryo before (top) and after (bottom) warping.

3, and 6 for **mindist1**, **mindist2** and **pointdist** respectively, and for the 9 day series: 7, 15 and 5.

The results of these reconstructions are shown in figures 8 and 9 which show both the registered and warped reconstructions of the 9 and 7.75 day embryos respectively. The top surface of each block in figure 8 shows a section taken in the original cutting direction; the other surfaces show orthogonal sections and a section cut in an arbitrary direction. From these images we see that warping has significantly improved the quality of the arbitrary section through the stack, and indeed, after warping the quality of an arbitrary section is similar to that of a section taken in the original cutting direction. Figure 9 shows the same section in a plane orthogonal to the cutting direction of the

7.75 day embryo before and after warping. We see that structures have become better differentiated and that the boundaries have become smooth. These results show that the requirements of the warping algorithm presented in this paper have been achieved.

4. Conclusion

The primary objective of the work described here was to develop a fully automatic technique for 3D reconstruction from serial section data. The aim was to produce a *representative* embryo for the purposes of a developmental atlas and gene expression database. There was no requirement to faithfully reproduce the originally sectioned embryo. The method had to cope with loss of alignment and sectioning distortions without the use of fiducials, and was required to produce a full 3D voxel image for the purpose of digital resectioning. We have been completely successful at achieving this objective, and in fact the first complete reconstructions, one from wax embedded material (a 9 day mouse embryo) and one from plastic sections (a 7.75 day embryo) are already in use.

In section 3 we showed that warping produces significant improvements over registration and that the resulting reconstruction is smooth, allowing proper resolution of structures in arbitrary planes. This was the primary objective of this work. Other methods for smoothing reconstructions have been presented in the literature, but most of these require that contours are (manually) extracted (Jansson 1994, Gérard *et al* 1993, Deverell *et al* 1993), and involve *removing data* to smooth the surfaces. The method presented here is fully automatic and does not remove any data. Furthermore, as required by the intended application, smoothing is of the entire grey level voxel image (thus smoothing both inner and outer surfaces) to enable arbitrary resectioning.

The underlying idea presented in this work is to model each section as a thin elastic plate, constrained so that points can move only within the plane of the plate. Forces are applied to each plate by matching corresponding points and the system is released and allowed to reach equilibrium. The material properties of each plate constrain the warp and preserve the biological structure. It was found that fine tuning of the parameters is not necessary in order to produce a satisfactory result. However care is needed when determining the distance between matchpoints (**pointdist**), the spring constant multiplier (**springk**), and the radius of the search area for correspondences (**areasize**), both to ensure convergence of the finite element iteration and to prevent unnecessary computation. **Pointdist** should be chosen sufficiently small to ensure a good result, but if computation time is an issue, the number of interesting points should be restricted. **Springk** should be chosen carefully because if it is too small, the sections will not be sufficiently warped to produce a smooth reconstruction, but if it is too large an inappropriate warp will occur. To avoid unnecessary computation, **areasize** should be chosen to be the minimum which will enable correct correspondences to be found. We note that **areasize** can be smaller than the maximum expected displacement.

Acknowledgments

The resources for this work, which forms part of a PhD project, were provided by the MRC Human Genetics Unit, and funding was provided by the SERC, the University of Edinburgh, and the parents of E Guest (with the help of the Dutch Government). The authors would like to thank Professor M Kaufman for making his section series of the 9-day embryo available, and Dr D Davidson and Alyson Ross for the 7-day plastic section series. Finally the authors wish to thank Dr G Robinson and Dr L Griffin for providing the code to produce a Delaunay triangulation from a set of points.

References

Andreason A, Drewes A M, Assentoft J E, and Larsen N E 1992 Computer-assisted alignment of standard serial sections without use of artificial landmarks. A practical approach to the utilization of incomplete information in 3-D reconstruction of the hippocampal region *J. Neurosci. Meth.* **45** 199–207

Apicella A, Kippenhan J S and Nagel J H 1989 Fast multi-modality image matching *Medical Imaging III: Image Processing (Proc. SPIE **1092**)* pp 252–63

Baldock R, Bard J, Kaufman M and Davidson D 1992 A real mouse for your computer *BioEssays* **14**

Bathe K-J 1982 *Finite Element Procedures in Engineering Analysis* (Englewood Cliffs, NJ: Prentice Hall)

Berthold C-H, Rydmark M and Corneliuson O 1982 Estimation of sectioning compression and thickness of ultrathin sections through vestopal-W-embedded cat spinal roots *J. Ultrastructure Res.* **80** 42–52

Deverell M H, Salisbury J R, Cookson M J, Holman J G, Dykes E and Whimster W F 1993 Three-dimensional reconstruction: Methods of improving image registration and interpretation *Analytical Cellular Pathology* **5** 253–62

Dürr R, Peterhans E and von der Heydt R 1989 Correction of distorted images pairs with elastic models *Eur. J. Cell Biol.* **48** Suppl. 25 85–88

Erricker B C 1971 *Advanced General Statistics* (London: Hodder and Stoughton)

Gérard H M, André J C and Mallet J L 1993 Computer-aided 3-D reconstructions from routine histologic sections *Microsc. Anal.* **33** 31–3

Guest] E 1994 Automatic Reconstruction from Serial Sections *PhD thesis* Department of Artificial Intelligence, University of Edinburgh

Hibbard L S, Grothe R A and Arnicar-Sulze T L 1993 Computed alignment of serial sections for 3-D reconstructions *Proc. SPIE* **1905** 946–55

Hibbard L S and Hawkins R A 1988 Objective image alignment for three-dimensional reconstruction of digital autoradiograms *J. Neurosci. Meth.* **26** 55–74

Jansson T 1994 Computerized alignment and deformation correction of microscopic serial section images of nervous tissue *Technical Report 257* School of Electrical and Computer Engineering, Chalmers University of Technology Göteborg, Sweden

Jones A S, Milthorpe B K and Howlett C R 1994 Measurement of microtomy induced section distortion and its correction for 3-dimensional histological reconstructions *Cytometry* **15** 95–105

Kaufman M H 1992 *The Atlas of Mouse Development* (London: Academic)

Kriete A 1989 Methodological basis of three-dimensional imaging and visualization in biomedical sciences—a review *MedTech '89: Medical Imaging (Proc. SPIE **1357**)* pp 2–13

Laan A C, Lamers W H, Huijsmans D P, te Kortschot A, Smith J, Strackee J and Los J A 1989 Deformation-corrected computer-aided three-dimensional reconstruction of immunohistochemically stained organs: Application to the rat heart during early organogenesis *The Anatomical Record* **224** 443–57

Lamers W H, Laan A C, Huijsmans D P, Smith J, Los J A and Strackee J 1989 Deformation-corrected computer-aided 3-D reconstruction of immunohistochemically stained sections of embryonic organs *Eur. J. Cell Biol.* **48** 103–6 Supplement 25

Lee D T and Schachter B J 1980 Two algorithms for constructing a delaunay triangulation *Int. J. Comput. Inform. Sci.* **9** 217–242

Montgomery K and Ross M D 1994 Improvements in semiautomated serial-section reconstruction and visualization of neural tissue from TEM images *Three-Dimensional Microscopy (Proc SPIE **2184**)* pp 264–7

Ogden R W 1984 *Non-Linear Elastic Deformations* (Chichester: Ellis Horwood)

Olivo J-C, Izpisúa-Belmonte J-C, Tickle C, Boulin C and Duboule D 1993 Reconstruction from serial sections: a tool for developmental biology. application to hox genes expression in chicken wing buds *Bioimaging* **1** 151–8

Preparata F P and Shamos M I 1985 *Computational Geometry: An Introduction* (Berlin: Springer)

Rees D W A 1990 *Mechanics of Solids and Structures* (New York: McGraw-Hill)

Richards J A, Sears F W, Wehr M R and Zemansky M W 1960 *Modern University Physics* (Reading, MA: Addison Wesley)

Ringwald M, Baldock R, Bard J, Kaufman M, Eppig J T, Richardson J E, Nadeau J H and Davidson D 1994 A database for mouse development *Science* **265** 2033–4

Rydmark M, Jansson T, Berthold C-H and Gustavsson T 1992 Computer-assisted realignment of light micrograph images from consecutive section series of cat cerebral cortex *J. Microsc.* **165** 29–47

Santori E M and Toga A W 1993 Superpositioning of 3-dimensional neuroanatomic data sets *J. Neurosci. Meth.* **50** 187–96

Stasa F L 1985 *Applied Finite Element Analysis for Engineers* (Tokyo, London: CBS International Editions)

Toga A W and Banerjee P K 1993 Registration revisited *J. Neurosci. Meth.* **48** 1–13

Verbeek F J 1992 Deformation correction using euclidean contour distance maps *Proc. 11th IAPR Int. Conf. on Pattern Recognition. Vol III Image, Speech and Signal Analysis* pp (IEEE Computer Society Press) pp 347–50

Yaegashi H, Takahashi T and Kawasaki M 1987 Microcomputer-aided reconstruction: a system designed for the study of 3-D microstructure in histology and histopathology *J. Microsc.* **146** 55–65

Zienkiewicz O C and Taylor R L 1989 *The Finite Element Method* vol 1 (New York: McGraw-Hill) 4th edn

—— 1991 *The Finite Element Method* vol 2 (New York: McGraw-Hill) 4th edn